Journal of Biomechanics 102 (2020) 109681

Contents lists available at ScienceDirect

Journal of Biomechanics

journal homepage: www.elsevier.com/locate/jbiomech
www.JBiomech.com

Estimating lumbar passive stiffness behaviour from subject-specific finite element models and in vivo 6DOF kinematics

Christian Affolter [a], Joanna Kedzierska [b], Thomas Vielma [c], Bernhard Weisse [a], Ameet Aiyangar [a,d,*]

[a] Mechanical Systems Engineering, EMPA-Swiss Federal Laboratories for Materials Science and Technology, Duebendorf, Switzerland
[b] DePuy Synthes GmbH, Oberdorf, BL, Switzerland
[c] Facultad de Ingeniería y Ciencias, Universidad Adolfo Ibáñez, Santiago, Chile
[d] Department of Orthopaedic Surgery, University of Pittsburgh, Pittsburgh, PA, USA

ARTICLE INFO

Article history:
Accepted 18 February 2020

Keywords:
Lumbar spinal loading
Subject-specific kinematics
Passive stiffness
Neutral position
Rigid-body musculoskeletal modelling

ABSTRACT

Passive rotational stiffness of the osseo-ligamentous spine is an important input parameter for estimating in-vivo spinal loading using musculoskeletal models. These data are typically acquired from cadaveric testing. Increasingly, they are also estimated from subject-specific imaging-based finite element (FE) models, which are typically built from CT/MR data obtained in supine position and employ pure rotation kinematics. We explored the sensitivity of FE-based lumbar passive rotational stiffness to two aspects of functional in-vivo kinematics: (a) passive strain changes from supine to upright standing position, and (b) in-vivo coupled translation-rotation kinematics. We developed subject-specific FE models of four subjects' L4L5 segments from supine CT images. Sagittally symmetric flexion was simulated in two ways: (i) pure flexion up to 12° under a 500 N follower load directly from the supine pose. (ii) First, a displacement-based approach was implemented to attain the upright pose, as measured using Dynamic Stereo X-ray (DSX) imaging. We then simulated in-vivo flexion using DSX imaging-derived kinematics. Datasets from weight-bearing motion with three different external weights [(4.5 kg), (9.1 kg), (13.6 kg)] were used. Accounting for supine-upright motion generated compressive pre-loads ≈ 468 N (±188 N) and a "pre-torque" ≈2.5 Nm (±2.2 Nm), corresponding to 25% of the reaction moment at 10° flexion (case (i)). Rotational stiffness estimates from DSX-based coupled translation-rotation kinematics were substantially higher compared to pure flexion. Reaction Moments were almost 90% and 60% higher at 5° and 10° of L4L5 flexion, respectively. Within-subject differences in rotational stiffness based on external weight were small, although between-subject variations were large.

1. Introduction

A lumbar segment's passive response is an important input parameter for spine musculoskeletal models. The flexion-extension stiffness is of particular importance, since flexion-extension is one of the most widely studied in vivo movements. These data are traditionally acquired from cadaveric testing (Gardner-Morse and Stokes, 2004; Goel et al., 1987; Heuer et al., 2007a; Panjabi et al., 1994; Stokes et al., 2002), wherein pure moments are applied on a functional spinal unit (FSU) to elicit rotation (Panjabi et al., 1994) in the presence of a superimposed, compressive 'follower load' (Patwardhan et al., 2003; Patwardhan et al., 1999). The *follower load* putatively represents the body weight acting axially on the spine during sitting or standing (Andersson et al., 1984; Gardner-Morse and Stokes, 2004), thus implicitly simulating coupled axial translational and rotational characteristics. However, in most cases, the superimposed follower load is of constant magnitude (Gardner-Morse and Stokes, 2004; Heuer et al., 2007a), which may not represent in vivo conditions (Beaucage-Gauvreau et al., 2019; Byrne et al., 2019 Kingma et al., 2016; Shirazi-Adl and Parnianpour, 2000). Although the superimposed axial load magnitude strongly influences passive rotational stiffness (Edwards et al., 1987; Gardner-morse and Stokes, 2003; Panjabi et al., 1977), rotational stiffness data under varying follower loads are sparse (Gardner-Morse and Stokes, 2004) and hence, seldom implemented in musculoskeletal models. Further, these datasets are limited to linearized behavior (Gardner-Morse and Stokes, 2004; Panjabi et al., 1976), hence may not represent behavior over finite rotations (O'Reilly et al., 2009).

Using subject-specific imaging-based finite element (FE) models built from CT/MR images obtained in the supine position is another increasingly common approach (Dreischarf et al., 2014;

* Corresponding author at: Mechanical Systems Engineering, EMPA-Swiss Federal Laboratories for Materials Science and Technology, Duebendorf, Switzerland.
E-mail address: ameet.aiyangar@empa.ch (A. Aiyangar).

https://doi.org/10.1016/j.jbiomech.2020.109681
0021-9290/

Liu et al., 2018; Naserkhaki and El-Rich, 2017). However, most studies tend to replicate the same, non-physiological boundary conditions of cadaver-based studies — pure rotational motion with a superimposed, constant follower load starting from a supine orientation.

Although the simulated dynamics from cadaveric tests may not be representative of in vivo conditions, they can serve as a fairly reliable calibration benchmark to optimize the *material properties* of the individual structures and sub-structures of the ligaments and intervertebral disk (IVD) needed to represent the FSU *stiffness* behavior (Schmidt et al., 2007; Weisse et al., 2012). In principle, provided an accurate 6DOF in vivo lumbar kinematics dataset were available, a calibrated FE model could then be driven with these kinematics to extract subject- and task-specific, FSU passive stiffness response. This alternative approach implicitly accounts for the varying coupled translational and rotational patterns occurring with the dominant rotational motion in question providing a task-specific passive response dataset, which is easily implementable in multi-body musculoskeletal models. This approach has theoretically become feasible, given the recent availability of directly measured in vivo lumbar vertebral kinematics obtained with x-ray fluoroscopy (Eskandari et al., 2017; Wu et al., 2014; Zanjani-Pour et al., 2018) and dynamic stereo X-ray (DSX) imaging techniques (Aiyangar et al., 2015; Aiyangar et al., 2014a). Indeed, variations of this approach have already been explored in recent studies (Dehghan-Hamani et al., 2019; Eskandari et al., 2017; Wang et al., 2014; Zanjani-Pour et al., 2018), although they were limited to static postures.

The current, feasibility study aims to compare the predicted flexion-extension stiffness responses of a lumbar FSU from the two aforementioned FE approaches driven by: (i) generic, pure flexion with a superimposed follower load, directly from the supine position, and (ii) in vivo flexion based on subject-specific DSX kinematics obtained during a dynamic lifting task. The study further explores the sensitivity of FE-derived passive rotational stiffness to two aspects of functional in-vivo kinematics related to case (ii): (a) accounting for passive strain changes from supine to upright standing position, and (b) coupled translation-rotation kinematics.

2. Materials and methods

The work was based on four subjects' data from a previous study (Aiyangar et al., 2014a). Subject-specific imaging-based FE models of individual L4L5 FSUs were generated based on CT images obtained in the supine state without external loading using a previously validated protocol (Weisse et al., 2012) with some modifications, as described below.

2.1. Mesh creation

The CT data were first segmented to isolate and create 3D vertebral surfaces from volumetric voxel data in *Mimics Innovation Suite v15.0* (*Materialise, Leuven, Belgium*). The STL-files were then exported to *TrueGrid®* (XYZ Scientific Applications, Inc., Livermore, CA, USA), a mesh pre-processor, to create a 3D FE mesh of hexahedral elements.

IVD geometry was based on adjacent vertebral endplate configuration obtained in the supine state, which served as the upper and lower disk faces. The disk mesh was fitted into the wedge-shaped space between two adjacent vertebrae using our previously developed protocol (Weisse et al., 2012). The protocol used mean values for the disk bulge, anterior-posterior (AP) nucleus pulposus offset and annulus radial thickness as a function of polar angle φ (Fig. 1, left). Thus, the IVD models were subject-specific with respect to endplate curvature and disk height, but not with respect to material properties, disk bulge and annulus fibre alignment.

The annulus comprised eight concentric layers meshed with 3D hexahedral elements, which made up the ground substance. A superimposed 'skin' was defined on each of the outer faces of these 8 solid layers (Fig. 1). The skin was meshed with membrane elements sharing the same nodes as the 3D hexahedral elements. Reinforcing fibre layers were embedded in the membrane layer. Previous implementation of a similar approach (Shirazi-Adl, 1988; Shirazi-Adl et al., 1984) with a composite membrane formulation was constrained to apply linear elastic material properties. In the current work, 'REBAR reinforcing elements' were applied to a homogenous shell (Simulia, 2016)) (Fig. 1, right). The *rebars* are considered analytically as a reinforcement of the membrane elements to allow nonlinear material property assignment to the anisotropic annulus layers.

Four lumbar ligaments were included in the models. Anterior (ALL) and posterior (PLL) longitudinal ligaments were represented with a 3D continuum mesh extruded from the vertebrae and IVD faces. The ligamentum flavum (FL) was modeled as a connector connecting the nodes from the lower end of L4 lamina to the upper

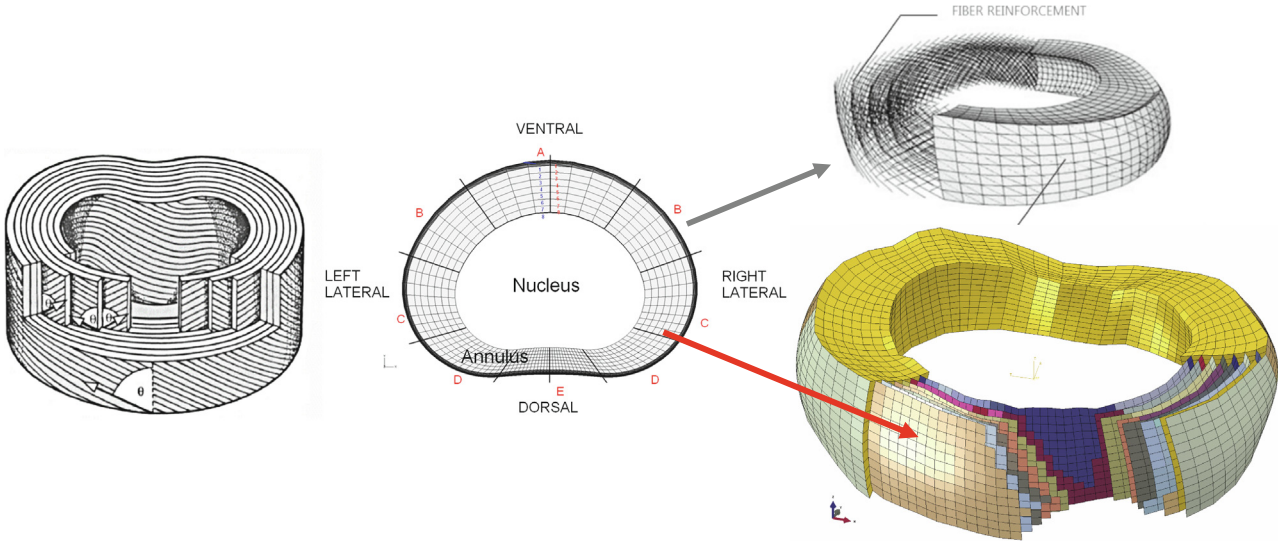

Fig. 1. Schematic description of IVD mesh creation. *left*: simplified lamellar layup of annulus with 8 layers; *middle*: scaled nucleus shape and sectors for fibre property assignment; *right*: two approaches for discretization of reinforcing fibres: discrete (top) and 'rebars' in membrane elements (bottom) [nucleus represented as a fluid cavity inside surface elements].

end of the L5 lamina. The supraspinous ligament (SSL) was modeled as a connector with nodes selected such that the connector was roughly tangential to the of L4 andL5 spinous processes. The intertransverse ligaments mainly contribute to lateral bending stiffness (Adams, 2006). (Zander et al., 2017) additionally showed that, of the seven ligaments, only LF, SSL, ALL and PLL influenced intra-diskal pressure (IDP), axial force and intervertebral rotations during flexion-extension, while the remaining three had a negligible influence. Hence, the remaining three ligaments were not modelled.

2.2. Component material properties

Locally varying transversely isotropic material properties were applied to the vertebral mesh elements based on CT-derived local apparent density (Hounsfield units), resulting in a heterogeneous and transversely isotropic Young's modulus distribution (Aiyangar et al., 2014b; Weisse et al., 2012). Facet joint contact was ignored as there was no contact during flexion motions, as shown in our recent work on mapping the in vivo facet joint kinematics from the same dataset (Byrne et al., 2018). Second, in the pure-flexion-with-follower-load case, the models, based on CT imaging datasets, did not show any facet contact during the range of flexion simulated. Hence, in both cases, we did not include facet contact definitions.

The nucleus pulposus was modelled as a fluid cavity in Abaqus/Standard 6.14, i.e. only the surrounding surface was meshed with surface elements. The cavity volume remained constant and the cavity pressure was a function of external load and resulting annulus deformation.

The annulus ground substance and superimposed membrane layer were assigned the same hyperelastic material properties. The reinforcing fibres (REBARS) were stiffer with nonlinear elasticity, and their volume content in the membrane elements represented the fibre volume content in the underlying solid layer.

ALL and PLL ligaments were modelled with hyperelastic material properties with Ogden 3rd order formulation (Table 1). The connector behaviour of SSL and LF were extracted from force vs. engineering strain curves (Chazal et al., 1985; Myklebust et al., 1988; Nolte and Pingel, 1991; Pingel, 1991; Shirazi-Adl et al., 1986). The slack length and stiffness were adjusted based on our previous work (Weisse et al., 2012) to reproduce, as best as possible, overall passive FSU behaviour reported in past published studies for pure flexion without follower load (Heuer et al., 2007b; Panjabi et al., 1994) and pure compression (Fagan et al., 2002; Lin et al., 1978). The supine posture was the starting configuration for these simulations. See Appendix A for additional detail on adjusting ligament slack length and stiffness.

2.3. Analysis models of the FSU

The different FSU models were set up by assembling the meshes of two adjacent vertebrae and the intermediate disk, and extending the model with the required ligaments. A typical model is shown in Fig. 2. As all the models had been meshed in the same global reference frame of the CT-based supine posture, the assembly process didn't require any alignment or translation of parts. After combining the meshes, the assembly was oriented such that the L5 reference frame was aligned with the global coordinate system (white arrows in Fig. 2). Two load cases of interest were analysed:

(1) Pure-flexion-with-follower-load:

The lower vertebra was fixed in space. A compressive, 500 N follower load was applied in the first step, with all rotational DOFs unconstrained. But first, in order to determine the optimal follower load direction such that no secondary bending or transverse displacements were generated, the follower load direction was iteratively adjusted until flexion rotation in the upper vertebra was almost zero ($\leq 0.1°$). Subsequently, the FSU was flexed with a rotation of 12° applied on the upper L4 vertebra. The constant 500 N force continued to be applied as a follower load. The resulting reaction moments and displacements were evaluated with respect to the L5 reference frame (white in Fig. 2).

(2) Dynamic-Stereo X-ray (DSX) based in vivo kinematics:

Four successive steps were applied as follows:

1. Simulate motion from supine, CT-based position to the static, upright DSX-based position *without* hand-held load. A linear, static ramp was implemented.
2. Simulate motion further to upright pose *with* hand-held load (load-bearing upright pose). Three separate simulations for each load case (4.5 kg, 9.1 kg, 13.6 kg) were implemented.
3. From static, load-bearing upright pose to end position of the lifting task as a linear ramp. This step was necessary, as the L4L5 configuration at the final, resting pose at the end of the lifting task did not necessarily match the configuration of the load-bearing upright pose, which was acquired separately. The described analysis is a motion-driven linear ramp between these postures.
4. Inverted extension (flexion) motion from the lifting task end position to the lifting task start position. The experimental lifting task was actually an extension motion (full-flexed position to upright position). Since this was a quasi-static simulation without accelerations or inertial effects, we assumed that the direction of simulation should not affect force and moment estimates.

Note: No additional follower load or any other external load was applied to the FE model in this case. The term "hand-held load" is meant to clarify the condition when kinematic measurements were made.

The following outputs were extracted and compared:

1. Compressive reaction force from DSX kinematics-based supine-to-upright motion was compared with the follower load of 500 N. The compressive reaction force is the reaction force along the vertical axis of the L5 reference coordinate system directly obtained as an output following FE simulation.

Table 1
Material parameters and references for the modelled ligaments.

Ligament	Ogden 3rd order parameters						References
	μ_1 D1	α_1 D2	μ_2 D3	α_2	μ_3	α_3	
ALL	0.177	3.08	0.627	−13.86	−0.357	−6.8	(Heuer et al., 2007; Nolte and Pingel, 1991; Pingel, 1991; Schmidt et al., 2007)
	1.0	1.0	1.0				
PLL	0.159	−1.126	0.77	−18.54	−0.39	−9.6	
	1.0	1.0	1.0				
SSL + LF	Force vs. elongation curves derived from Force-strain curves presented in cited publications.						(Chazal et al., 1985; Myklebust et al., 1988; Nolte et al., 1990; Nolte and Pingel, 1991; Shirazi-Adl et al., 1986)

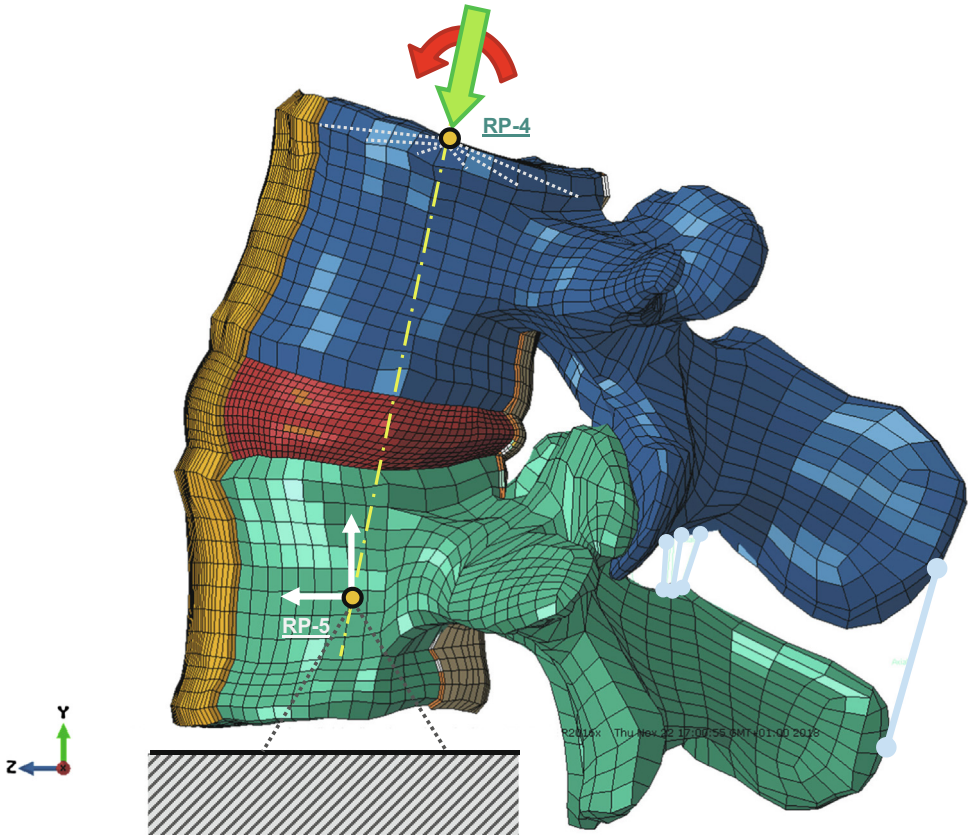

Fig. 2. Analysis model of an L4-L5 FSU.

2. IDP and compressive reaction force were compared with published in vivo IDP (Wilke et al., 2001).
3. Reaction moment vs. rotation curves from pure-flexion-with-follower-load case were compared with corresponding curves from the DSX-driven models. The reaction moment is an output directly obtained following FE simulation at the L4 reference point in the parent, L5 reference coordinate system.
4. Shear reaction forces from kinematic data-driven models. This is the AP component of the reaction force at the defined reference point of L5 with respect to its reference frame and obtained directly as an output following FE simulation.

3. Results

Simulating the transition from supine (CT orientation) to upright (DSX kinematics) pose resulted in a mean compressive reaction force of 468 N (±188 N) for the first three subjects (Fig. 3, bottom). The corresponding mean (±S.D.) IDP value was 0.4 MPa (±0.1 MPa) (Fig. 3, top; Table 2). One subject (subject # 4) resulted in negative IDP (−0.05 MPa) and compressive reaction force – a notable exception and a rather counter-intuitive result. Simulating further from the upright, no-load state to the upright configurations with hand-held load resulted in an increase in the IDP and corresponding compressive reaction force, although subject #4 continued to be an exception in this regard. While the general trend (for subjects 1–3) was an increasing IDP with increasing hand-held load, as observed based on the averaged results, this was not always the case. For example, IDP was highest in the 4.5 kg configuration for subject #2, and in the 9.1 kg configuration for subject #3.

Predicted IDP values over the simulated continuous motion exhibited substantial variability (Fig. 4). While three out of the four subjects' IDP generally displayed an increasing trend, IDP for subject #3 exhibited a counter-intuitive decrease by a factor of ~0.4 towards the end (flexed position) of the simulated motion compared to the upright position.

The associated mean AP shear reaction force over the range of motion was between 75 and 125 N (Fig. 5), which compares favourably with those reported previously (Arshad et al., 2017).

Regarding rotational components, simulating pure flexion with a constant, 500 N follower load resulted in a mean reaction moment of 10 Nm (±4 Nm) at 10° flexion (Fig. 6). This matched well with the flexion-extension stiffness (10 ± 2.4 Nm/° for this case reported by (Gardner-Morse and Stokes, 2004), assuming linearized stiffness. However the curves were, expectedly, nonlinear, similar to previous studies (Heuer et al., 2007b; Naserkhaki et al., 2016; Panjabi et al., 1994).

For DSX-based models, in addition to a compressive reaction force, going from supine to upright standing also generated a non-zero mean flexion moment of 2.5 Nm (±2.2 Nm). In contrast to the compressive force, this "pre-torque" was relatively less sensitive to the magnitude of hand-held load. While the nonlinear curves obtained using DSX-based kinematics exhibited similar patterns to the pure-flexion-with follower-load case, the passive behaviour was substantially stiffer on average. Further, differences due to weight lifted were much smaller compared to variability across subjects.

4. Discussion

The study explored the feasibility of estimating a lumbar segment's rotational (flexion-extension) passive stiffness behaviour from FE models driven with subject-specific, in vivo coupled rotation-translation kinematic data. While the models were based

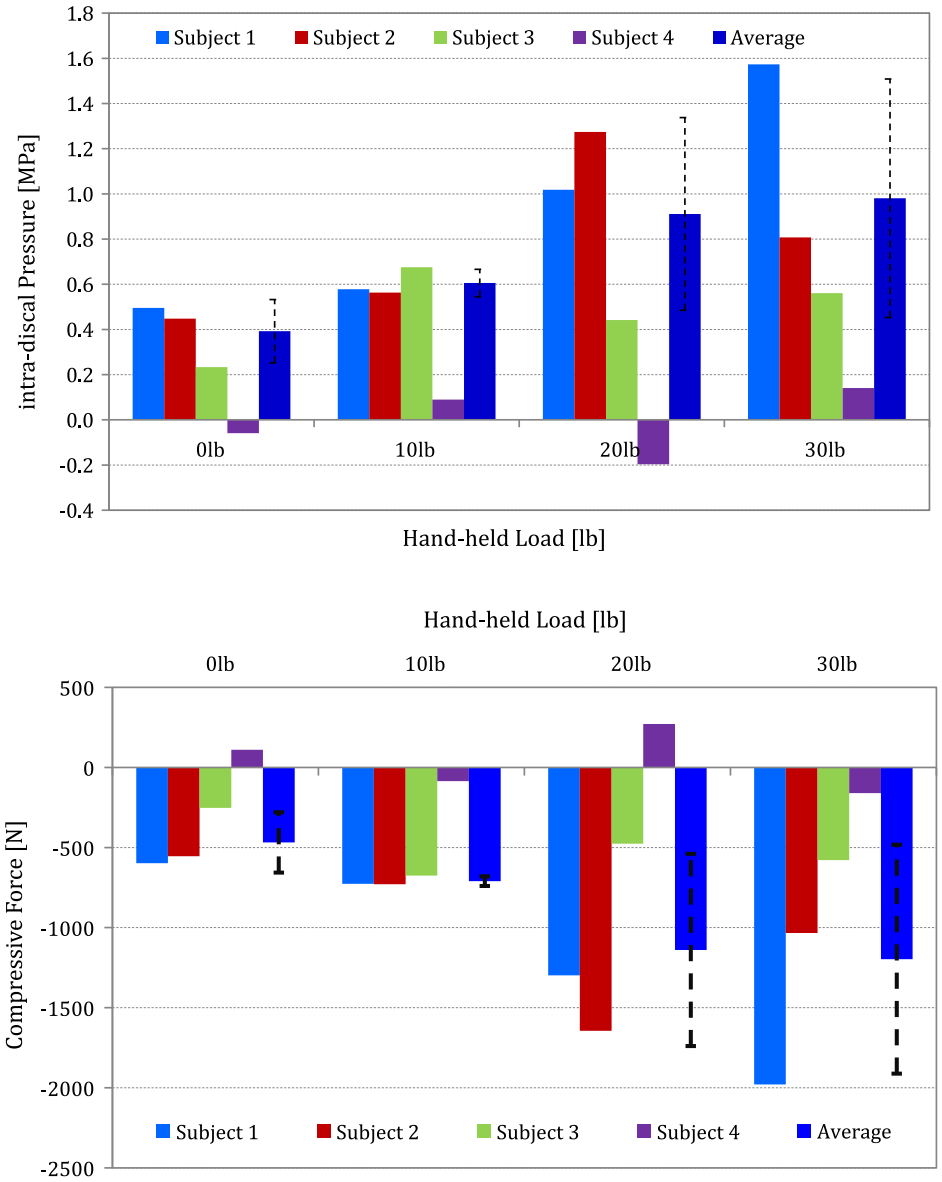

Fig. 3. Top: Intra-diskal pressure (IDP values) at upright position. Bottom: Compressive force generated at upright position. Error bars are standard deviations. Mean values are based on average from subjects 1, 2 and 3 (Subject 4 is considered an outlier).

Table 2
Subject body mass in kg and intra-diskal pressure (IDP) values in MPa at upright position for different hand-held loads. The mean, standard deviation and coefficient of variation calculations are based on subjects 1, 2 and 3. For these purposes, subject 4 is considered an outlier.

Subject #		Intra-diskal pressure (IDP) in upright stance with different hand-held Loads			
	Subject Mass (kg)	0 kg IDP (MPa)	4.54 kg IDP (MPa)	9.1 kg IDP (MPa)	13.6 kg IDP (MPa)
1	84.2	0.5	0.58	1.02	1.57
2	74	0.45	0.56	1.27	0.81
3	60.8	0.23	0.68	0.44	0.56
4	67.4	−0.06	0.09	−0.20	0.14
Mean (1–3)	71.6	0.4	0.61	0.91	1.0
Standard Deviation (1–3)	11.7	0.14	0.06	0.43	0.53
Coefficient of Variation (1–3)	16%	35%	10%	46%	53%

on subject-specific vertebral CT-geometry, the input kinematics were based on 6DOF kinematics of the individual vertebrae recorded using DSX imaging of an in vivo functional lifting task, wherein the transition from supine to upright pose was additionally considered. These results were compared to the corresponding behaviour with an input of pure flexion under a constant follower load, starting from a supine configuration.

While no comprehensive validation studies were performed for the DSX kinematics-based simulations — there are very few studies against which to benchmark our results — IDP in upright standing,

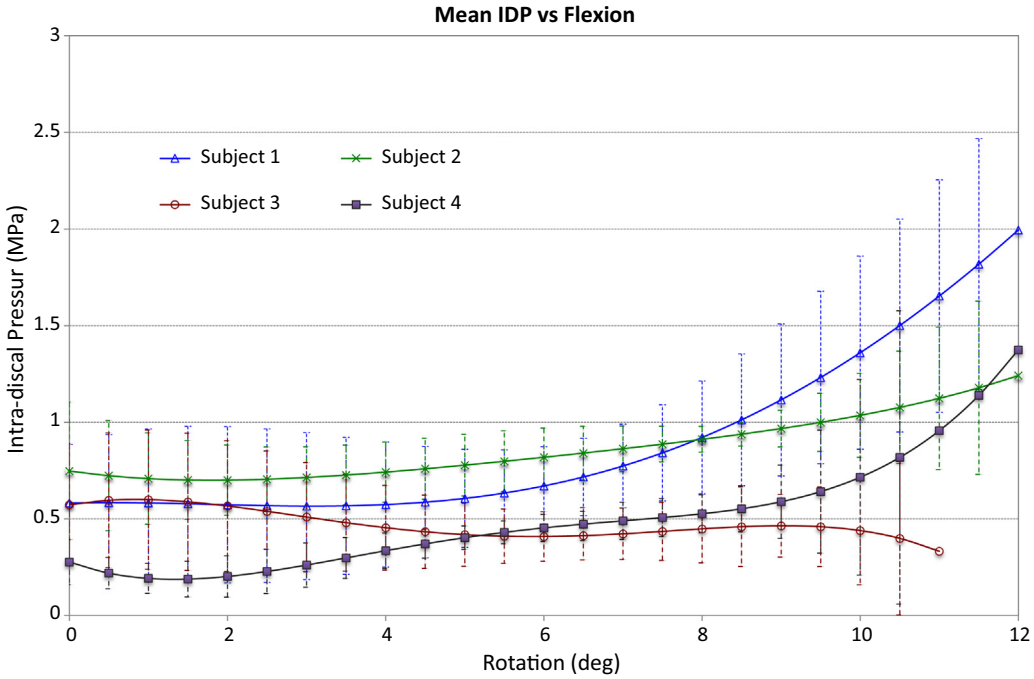

Fig. 4. Intra-diskal pressure IDP over the inverted lifting task (simulated flexion) based on the DSX kinematic dataset. Each subject's curve is an average over the three hand-held loads during the lifting tasks. Error bars are standard deviations.

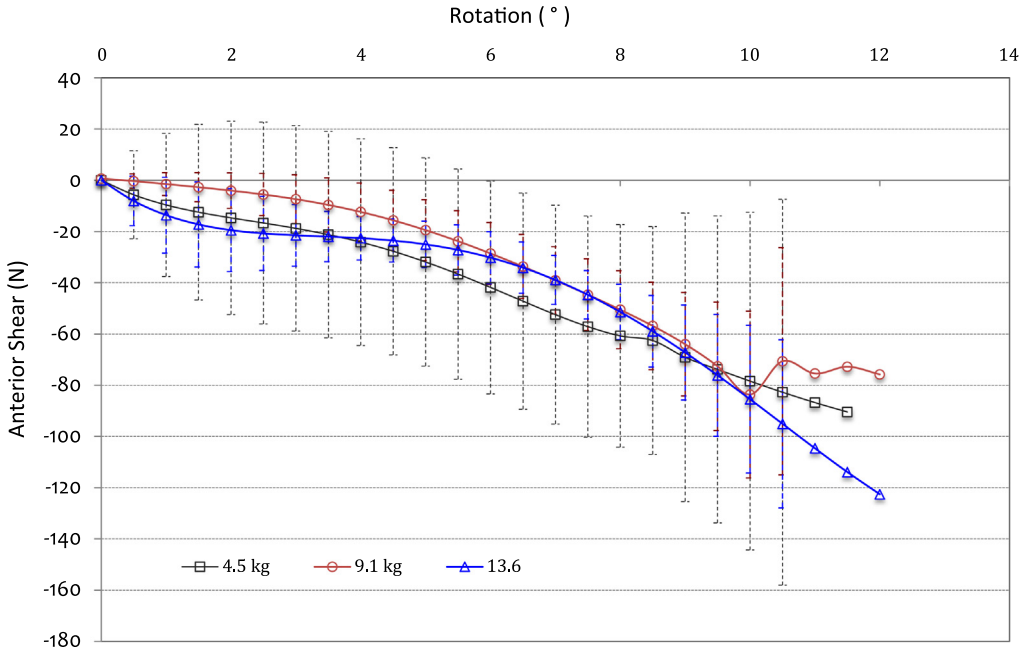

Fig. 5. Anterior-posterior shear forces (relative change from upright posture). Each curve represents the average of the four subjects tested. Error bars are standard deviations.

and IDP and coupled shear over the DSX-based *inverted extension* were compared against past studies (Arshad et al., 2017; Gardner-Morse and Stokes, 2004; Sato et al., 1999; Takahashi et al., 2006; Wilke et al., 2001). The results, which should be considered preliminary, highlight potential positives of using this approach, but they also reveal some significant pitfalls.

On the positive side, and with regard to the main goal of obtaining flexion-extension passive behaviour, the DSX kinematics-based results differed from the pure-flexion-with-follower-load results in two ways. First, going from supine to upright not only generated a compressive reaction force, but also a reaction moment. This "pre-torque" — approximately 25% of the reaction moment attained at 10° flexion in the pure-flexion-with-follower-load case (Fig. 6) — is not insubstantial. (Dehghan-Hamani et al., 2019) recently noted that going from supine to upright not only alters the translational kinematics, but also the rotational kinematics. This "pre-torque" is a manifestation of the altered rotational configuration. Furthermore, the mean reaction moment was 3 Nm (±1.4 Nm) – approximately 90% – and 6 Nm (±3 Nm) – approximately 60% – larger at 5° and 10° flexion, respectively. Thus, the in vivo passive flexion-extension response with coupled rotation-translation kinematics can be much stiffer than that estimated based on pure flexion, even with a superimposed follower load.

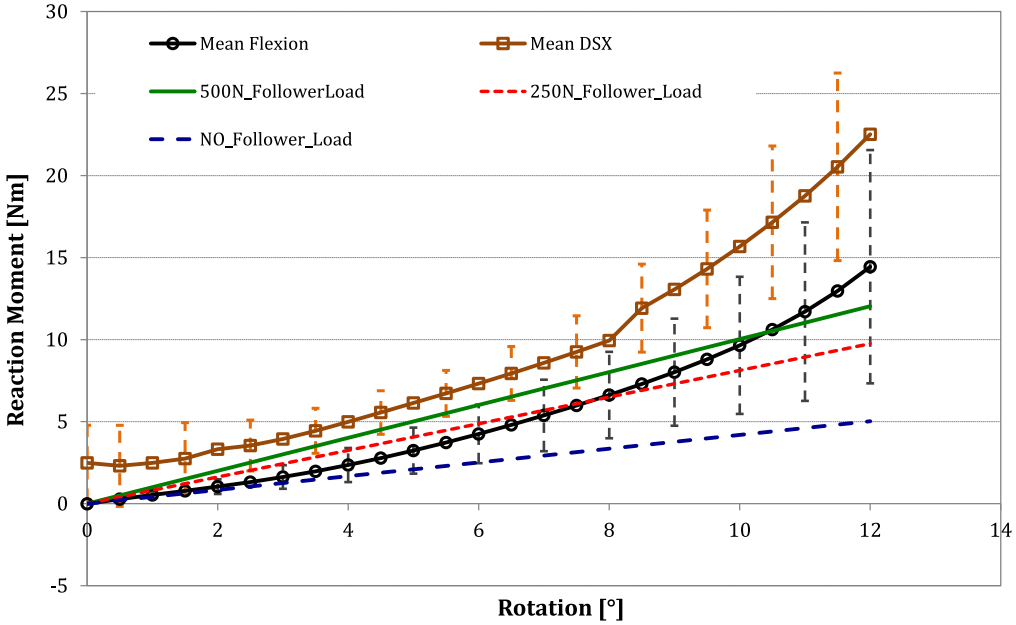

Fig. 6. Average reaction moment vs. flexion rotation curves for the two cases tested. The reaction moment is an output directly obtained following FE simulation at the L4 reference point in the parent, L5 reference coordinate system. (a) Pure flexion with follower load (mean_flexion) and (b) Dynamic-Stereo X-ray (DSX) based in vivo Kinematic dataset (mean_DSX). Error bars are standard deviations. Three linear curves represent equivalent reaction moment-flexion relationship based on stiffness values reported by Gardner-Morse et al. 2004 for three different follower loads: 0 N (NO_Follower_Load); 250 N (250N_Follower_Load) and 500 N (500 N Follower Load).

Further on the positive side, momentarily leaving aside the rather counter-intuitive negative IDP results from subject #4, IDP estimates ($\bar{x}$ = 0.4 MPa, Range: 0.23–0.5 MPa) in the upright pose without load compare quite favourably to previous, experimentally recorded in vivo values [0.49 MPa, single subject (Wilke et al., 2001); $\bar{x}$ = 0.35 MPa (Takahashi et al., 2006); and $\bar{x}$ = 0.5 MPa, Range: 0.22–0.75 MPa (Sato et al., 1999)]. This more-or-less held true for the upright pose with hand-held load as well: mean IDP for the largest hand-held load case was larger than the corresponding no-load case value by a factor of 2.5 (±0.7), which is reasonable compared to the increase reported by Wilke et al. (*~2.1x*).

The corresponding mean compressive reaction force, obtained from the FE simulation driven purely with kinematic inputs without including any representation of external loads or subject body weight, was remarkably similar to the 500 N follower load applied in in-vitro testing and FE models, and assumed to represent combined muscle and gravity loads in the upright position (Andersson et al., 1984; Azari et al., 2018; Gardner-Morse and Stokes, 2004). Although inter-subject variability was substantial, the variability was well within the range reported in previous in vivo measurements (Sato et al., 1999). Similarly, albeit with a couple of exceptional instances, the general trend of increasing compressive reaction force for upright standing with progressively larger hand-held loads (0–4.5–9.1–13.6 kg) provides further confidence for this approach.

Predicted IDP values over the simulated continuous motion, however, did not always follow the expected trend – a monotonic increase in IDP with flexion (Wilke et al. 2001). Overall, IDP increased by a factor of 2.6 (±1.6) on average over the range of simulated flexion (inverted extension) motion, compared to a factor of 2.3 reported by (Wilke et al., 2001) for a stoop lift. This comparison is reasonable, as the lifting task was basically a stoop lift, i.e. without knee-bending and starting from ~75° trunk-flexed pose (Aiyangar et al., 2014a). Nevertheless, the patterns and magnitude of increase over the motion varied substantially across subjects.

Finally, coupled AP shear reaction forces were also within range of previously reported values (Arshad et al., 2017; Ghezelbash et al., 2016).

On the other hand, the two unexpected results for IDP — negative IDP (−0.05 MPa) for subject #4 in upright standing and IDP decreasing by a factor of ~0.4 for subject #3 during continuous motion — raise valid concerns regarding the robustness of this approach. The following points need to be considered.

First, a zero initial stress state (null IDP) was assumed for the supine position, although studies have shown that IVDs exhibit a non-zero pressure of ~0.1 MPa (Wilke et al., 1999). Second, two separate imaging modalities were used to obtain L4-L5 FSU configurations in the supine and upright positions: CT imaging (resolution 0. 25 mm × 0.25 mm × 1.25 mm reconstructed to 0.25 mm^3 voxels) and DSX imaging (accuracy ≤ 0.26°; 0.2 mm) for supine and upright configurations, respectively. Thus one must reckon with a potential cumulative error between 0.2 and 0.4 mm, at least, in estimating supine-to-upright transition. Third, axial compressive stiffness estimates of L4L5 FSUs lie between 2000 and 2500 N/mm (Fagan et al., 2002; Gardner-Morse and Stokes, 2004; Senteler et al., 2015). Hence axial force and corresponding IDP estimates can be quite sensitive to small errors in axial displacement. (Dehghan-Hamani et al., 2019) recently showed that just altering axial displacement by ±0.1 mm changed IDP by ~0.2 MPa. By contrast, stiffness estimates in shear direction are between 10 and 25% of axial stiffness (Dehghan-Hamani et al., 2019; Gardner-Morse and Stokes, 2004; Senteler et al., 2015), implying force outputs would be correspondingly much less sensitive to AP translational errors of similar magnitude. Further, (Dehghan-Hamani et al., 2019) additionally showed that IDP was even less sensitive to rotation errors: ± 3° error (*>10x rotational accuracy of DSX system*) altered IDP by less than 10%. Thus, a cumulative error of 0.2 mm in estimating the axial displacement between the two positions could potentially completely erase the IDP expected in the upright stance, while AP shear and presumably the flexion reaction moment would likely be much less affected. In the particular case of subject #4, IDP for all four cases of upright standing were much closer to zero (Fig. 3, Table 2), which suggests the dominant common underlying cause of low IDP was likely an erroneous underestimation of IVD height in CT-derived supine configuration.

The second counter-intuitive result was the decreasing IDP ($\bar{x}$ = 0.57 to 0.33 MPa) for subject #3 over the continuously

simulated motion. To the authors' knowledge, only one other study explicitly accounting for 6DOF biplane fluoroscopy based kinematics used a similar approach and reported lower IDP estimates in the flexed pose compared to upright (Wang et al., 2014). Unfortunately an explanation for their observation was missing. While accuracy limits of the imaging modalities could also partly explain the decrease in our study, they do not fully explain the decrease over the range of motion, which comprises data captured over 60 frames and two seconds (Aiyangar et al., 2014a). This implies, and we speculate, that there was likely an additional bias in (over)estimating IVD height, however small, in flexed configuration compared to the upright configuration. Again, while these small errors clearly significantly affect IDP estimates, resulting in counter-intuitive decreases in IDP from upright to flexed stance, the AP shear estimates or the flexion-extension reaction moment are likely much less sensitive.

Nevertheless, these two counter-intuitive results, together, highlight potential pitfalls of this approach. Results from a recent Monte Carlo-based simulation study (Eskandari et al., 2019) appear to confirm the "hypersensitivity" of IDP predictions to errors in image-based kinematics. For instance, the study reported large coefficients of variation (CV) in IDP estimates in relaxed upright standing — between 30%–77% and 74%–148% from their passive FE and musculoskeletal model-based simulations respectively — from relatively small, translation errors between 0.1 and 0.3 mm induced into the models, which were constructed from a single subject's CT images. In comparison, CVs of IDP estimates from the current study are lower — 10%–53% —, of which at least 16% could be attributed to the variability between subjects (Table 2). Thus, these initial results with this approach show promise. Nevertheless, the works of Eskandari et al., Dehghan-Hamani et al. and particularly the counter-intuitive IDP results from the current study suggest caution in adopting this approach.

Other limitations include the following. First, the initial IVD bulge in supine position was assumed and not explicitly based on subject-specific imaging. Although the soft tissue component passive properties of the FSU were adjusted to reproduce overall flexion behaviour reported in cadaveric- and associated FE studies (Heuer et al., 2007b; Panjabi et al., 1994; Schmidt et al., 2006), these are, self-evidently, not subject-specific properties. The small sample size — single FSU each from four subjects — is another limitation. However, this initial study was mainly designed to explore the feasibility of this approach. We intend to continue to apply this approach to a larger available dataset comprising more subjects and more segment levels (L2-S1), to investigate if the counter-intuitive results seen in this study are simply outliers or if they are more widely prevalent, thus limiting the potential benefits of this approach due to the high sensitivity to axial translations. Finally, the intended main result—the flexion-extension passive behaviour— indicated a stiffer response for the subject- and task-specific DSX kinematics-based input compared to the pure-flexion-with-follower load case. It remains to be seen how strongly this difference influences joint loading estimates obtained from multi-body musculoskeletal models incorporating these properties, which is also the focus of a follow-up future study.

Declaration of Competing Interest

The authors have no conflict of interest (e.g. consultancies, stock ownership, equity interests, patent-licensing arrangements) related to the manuscript or the work it describes.

Acknowledgements

This work was supported by an *Ambizione Career Grant Award* (PZ00P2_154855/1) from the Swiss National Science Foundation (SNSF). Authors would like to acknowledge Ms Hajer Zouinekh for assistance with meshing and setting up some of the finite element models used in this study, and for compiling the results.

Appendix A. Calibration of ligament properties

Ligament properties were calibrated in order to reproduce passive flexion behavior of the L4-L5 FSU reported by in-vitro cadaveric studies (Heuer et al., 2007a, 2007b; Panjabi et al., 1994) in the current FE model. Calibration of ligament properties was initiated after IVD material properties were optimized based on the work of (Schmidt et al., 2006) and reported in detail in our previous publication (Weisse et al., 2012). Fig. A1, below, shows the final, optimized behavior of a representative L4-L5 IVD without ligaments and facets in comparison with the IVD passive behavior reported by (Schmidt et al., 2006).

In general, the ligament load-deformation curves in tension bear a sigmoidal shape (Chazal et al., 1985) (Fig. A2) – an initial nonlinear, concave zone, followed by a linear portion eventually culminating in a final downward-shaped nonlinear zone when the ligament experiences mechanical failure. The first two zones were considered for optimizing ligament properties. The first zone, wherein the ligament exhibits a finite amount of deformation with little increase in reaction force was modeled using an exponential form (Nolte et al., 1990) as follows:

$y = P(e^{Kx} - 1)$: Where y = ligament force; x = ligament deformation; P, K are constants to be determined.

The linear region is modeled as $= k(x - l_O)$: *where k = linear stiffness; l_O = x-intercept obtained by extending the linear portion of the curve down to the abscissa* (Fig. A2).

An initial assumption took the total deformation of the nonlinear, exponential part to be 1.66 l_O, with an initial value of 1 mm for l_O. The junction point, A, is the point where the value of the slopes of the nonlinear, exponential curve and the linear portion are equal. This was used to solve for the constants, P and K, in Matlab (Mathworks Inc., Natick, MA, USA), based on the equations shown below.

$$slope\ \ (linear\ \ portion) = k;\ \ Diagonal = \left(\frac{2}{3}l_o\right)\sqrt{1+k^2}; d$$
$$= Deformation\ \ at\ \ "A";\ \ f = Force\ \ at\ \ "A"$$

$$x\ \ coordinate\ \ of\ \ point\ \ A = l_o + \frac{2}{3}l_o;\ \ y\ \ coordinate\ \ of\ \ A = f$$
$$= k * \frac{2}{3}l_o$$

$$y = P\left(e^{Kx} - 1\right) \rightarrow K = \frac{\ln\left(\frac{y}{P} + 1\right)}{x}$$

Taking the first derivative of "y" with respect to "x", we get; $\frac{dy}{dx} = PKe^{Kx}$

This is also the slope of the load-deformation curve. The value of this slope at x = "d" is "k", the stiffness of the linear portion of the curve:

$$\frac{dy(d)}{dx} = k = P\left(\frac{\ln\frac{f}{P} + 1}{d}\right)\left(\frac{f}{P} + 1\right)$$

The equation is used to solve for "P" and "K" in Matlab.

This initial assumption still resulted in a very stiff behavior of the ligaments and, consequently, the FSU in flexion as compared to (Heuer et al., 2007a, 2007b). Hence, in order to introduce more compliance to the ligaments, particularly to the Ligamentum

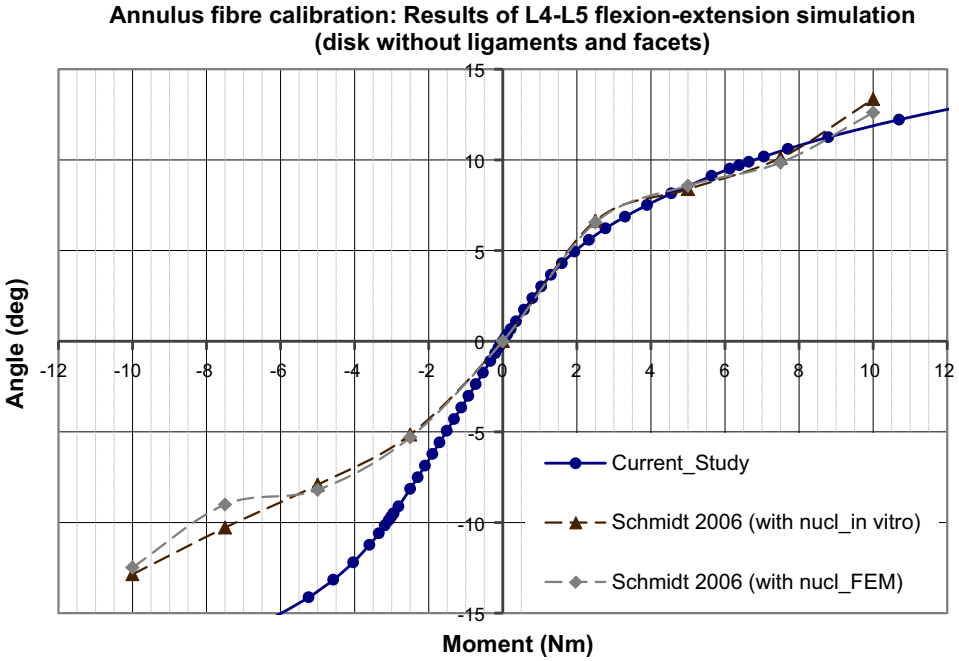

Fig. A1. Comparison of FE model passive flexion-extension behavior of the FSU without ligaments and facet joint contact from the current study with those reported by Schmidt et al., 2006. The curve represents the passive behavior of the FE model used in the current study after optimizing the IVD material properties.

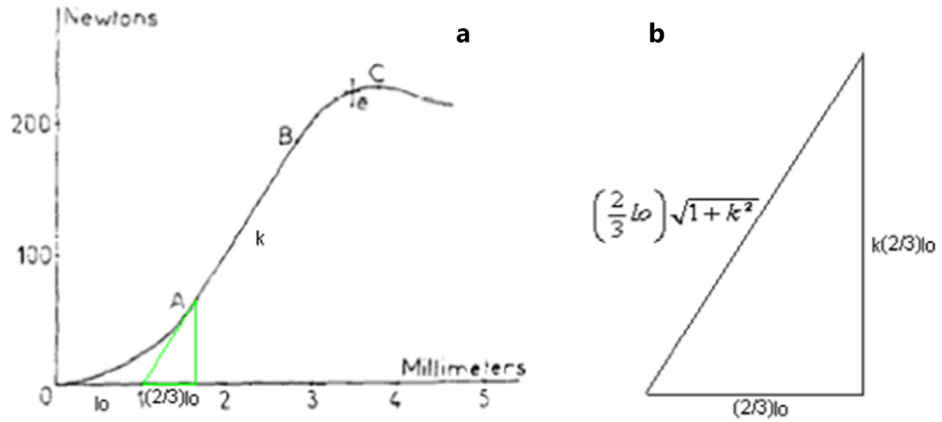

Fig. A2. (a) Schematic of load-deformation curve for a spinal ligament exhibiting the sigmoidal shape [from (Chazal et al., 1985)]. Figure also shows the estimation of "l_0" based on extending the linear portion of the curve down to the x-axis (b).

Flavum (LF) and the Supraspinous ligament (SSL), we increased the value of l_0 and also added an additional "slack" zone to the initial part of the curve wherein the ligaments undergo a finite deformation without developing any reaction force, as shown below in Fig. A3. This was based on results reported by (Shirazi-Adl et al., 1986), wherein the slack lengths were much greater than the 1 mm used in initially in this study. The "slack" zone (part where elongation of ligament generates no force) was set to 70% of l_0. The exponential zone then extended from 0.7 l_0 to 1.2 l_0, from where the linear zone extended further. This change is illustrated below. The equation used to find K and P were also adjusted accordingly, as below. (os = 0.7 l_0)

$$K = \frac{\ln(\frac{y}{P}+1)}{x-os};\ 0 = P\left(\frac{\ln\left(\frac{f}{P}+1\right)}{d-os}\right)\left(\frac{f}{P}+1\right) - k$$

l_0 was iteratively adjusted until a good match was achieved between the simulated flexion behavior and the benchmarked in-vitro behavior reported by (Heuer et al., 2007a, 2007b). l_0 for LF and SSL were set between 3 mm and 5 mm for the various subjects' FSUs modeled in the current study. Given that, according to (Nolte and Pingel, 1991; Shirazi-Adl et al., 1986), the neutral zone of SSL and LF can extend up to 30% of strain, and that average lengths for LF and SSL have been reported as 22 mm and 30 mm respectively, the final values for l_0 appear reasonable. The shape of the ligament load-deformation curves were modified until the overall FSU behavior lay within the range reported by Heuer et al., 2007, and Panjabi et al., 1994. Fig. A4 below shows the improvement in matching flexion behavior of the L4-L5 FSU of one of the subjects from the current study with the in-vitro flexion behavior reported by Heuer et al., 2007a, 2007b.

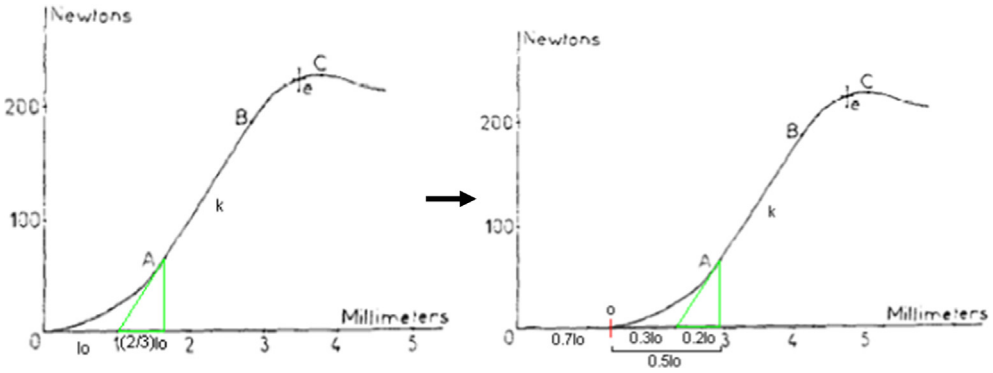

Fig. A3. Modification of sigmoidal ligament load-deformation curve to modify the slack length.

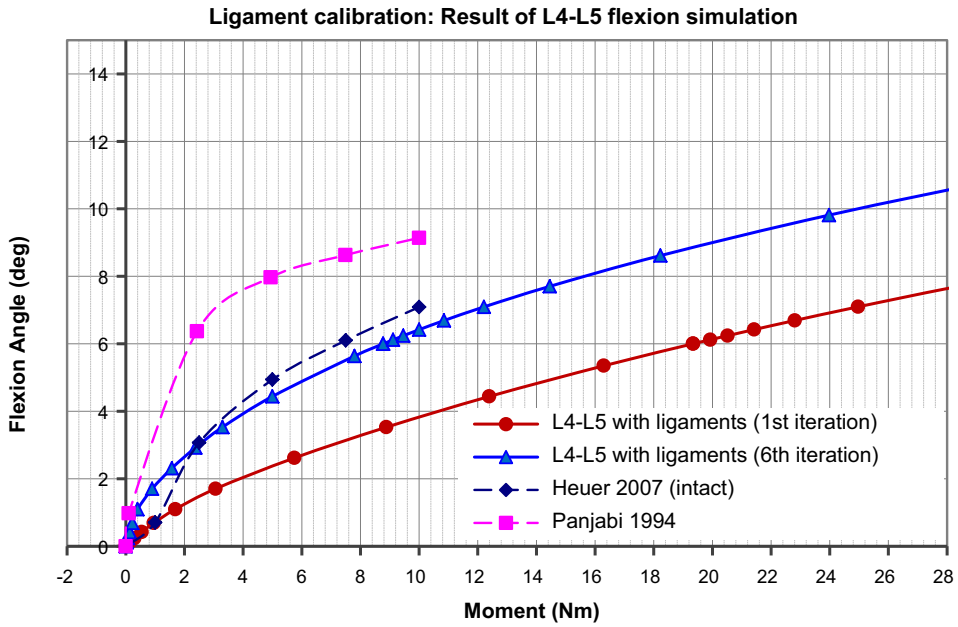

Fig. A4. Calibration of flexion stiffness in a representative L4-L5 FSU. 1st iteration shows stiff behavior. Iteratively adjusting slack length and stiffness of the ligaments (SSL and LF) brings the overall FSU stiffness closer to published in-vitro studies (Heuer et al., 2007; Panjabi et al., 1994) by the 6th iteration. In this case, the stiffness behavior is tuned to match results of Heuer et al., 2007a, 2007b.

References

Adams, M., Bogduk, B., Burton, K., Dolan, P., 2006. The Biomechanics of Back Pain. Churchill Livingstone, New York, NY.

Aiyangar, A., Zheng, L., Anderst, W., Zhang, X., 2015. Apportionment of lumbar L2–S1 rotation across individual motion segments during a dynamic lifting task. J. Biomech. 48, 3709–3715.

Aiyangar, A., Zheng, L., Tashman, S., Anderst, W., Zhang, X., 2014a. Capturing three-dimensional in vivo lumbar intervertebral joint kinematics using dynamic stereo-X-ray imaging. J. Biomech. Eng. 136.

Aiyangar, A.K., Vivanco, J., Au, A.G., Anderson, P.A., Smith, E.L., Ploeg, H.L., 2014b. Dependence of anisotropy of human lumbar vertebral trabecular bone on quantitative computed tomography-based apparent density. J. Biomech. Eng. 136.

Andersson, G.B., Chaffin, D.B., Pope, M.H., 1984. Occupational biomechanics of the lumbar spine. Praeger, New York, Occupational low back pain, p. 45.

Arshad, R., Zander, T., Bashkuev, M., Schmidt, H., 2017. Influence of spinal disc translational stiffness on the lumbar spinal loads, ligament forces and trunk muscle forces during upper body inclination. Med. Eng. Phys. 46, 54–62.

Azari, F., Arjmand, N., Shirazi-Adl, A., Rahimi-Moghaddam, T., 2018. A combined passive and active musculoskeletal model study to estimate L4–L5 load sharing. J. Biomech. 70, 157–165.

Beaucage-Gauvreau, E., Robertson, W.S.P., Brandon, S.C.E., Fraser, R., Freeman, B.J.C., Graham, R.B., Thewlis, D., Jones, C.F., 2019. Validation of an OpenSim full-body model with detailed lumbar spine for estimating lower lumbar spine loads during symmetric and asymmetric lifting tasks. Comput. Methods Biomech. Biomed. Eng. 22, 451–464.

Byrne, R.M., Zhang, X., Aiyangar, A.K., 2019. Sensitivity of musculoskeletal model-based lumbar spinal loading estimates to type of kinematic input and passive stiffness properties. 3rd International Workshop on Spine Loading and Deformation. Berlin, Germany.

Byrne, R.M., Zhou, Y., Zheng, L., Chowdhury, S.K., Aiyangar, A., Zhang, X., 2018. Segmental variations in facet joint translations during in vivo lumbar extension. J. Biomech. 70, 88–95.

Chazal, J., Tanguy, A., Bourges, M., Gaurel, G., Escande, G., Guillot, M., Vanneuville, G., 1985. Biomechanical properties of spinal ligaments and a histological study of the supraspinal ligament in traction. J. Biomech. 18, 167–176.

Dehghan-Hamani, I., Arjmand, N., Shirazi-Adl, A., 2019. Subject-specific loads on the lumbar spine in detailed finite element models scaled geometrically and kinematic-driven by radiography images. Int. J. Numer. Methods Biomed. Eng., 35

Dreischarf, M., Zander, T., Shirazi-Adl, A., Puttlitz, C.M., Adam, C.J., Chen, C.S., Goel, V. K., Kiapour, A., Kim, Y.H., Labus, K.M., Little, J.P., Park, W.M., Wang, Y.H., Wilke, H.J., Rohlmann, A., Schmidt, H., 2014. Comparison of eight published static finite element models of the intact lumbar spine: predictive power of models improves when combined together. J. Biomech. 47, 1757–1766.

Edwards, W.T., Hayes, W.C., Posner, I., White III, A.A., Mann, R.W., 1987. Variation of lumbar spine stiffness with load. J. Biomech. Eng. 109, 35–42.

Eskandari, A.H., Arjmand, N., Shirazi-Adl, A., Farahmand, F., 2017. Subject-specific 2D/3D image registration and kinematics-driven musculoskeletal model of the spine. J. Biomech. 57, 18–26.

Eskandari, A.H., Arjmand, N., Shirazi-Adl, A., Farahmand, F., 2019. Hypersensitivity of trunk biomechanical model predictions to errors in image-based kinematics when using fully displacement-control techniques. J. Biomech. 84, 161–171.

Fagan, M.J., Julian, S., Siddall, D.J., Mohsen, A.M., 2002. Patient-specific spine models. Part 1: Finite element analysis of the lumbar intervertebral disc—a material sensitivity study. Proc. Inst. Mech. Eng 216, 299–314.

Gardner-morse, M.G., Stokes, I.A., 2003. Physiological axial compressive preloads increase motion segment stiffness, linearity and hysteresis in all six degrees of freedom for small displacements about the neutral posture. J. Orthop. Res. 21, 547–552.
Gardner-Morse, M.G., Stokes, I.A.F., 2004. Structural behavior of human lumbar spinal motion segments. J. Biomech. 37, 205–212.
Ghezelbash, F., Shirazi-Adl, A., Arjmand, N., El-Ouaaid, Z., Plamondon, A., 2016. Subject-specific biomechanics of trunk: musculoskeletal scaling, internal loads and intradiscal pressure estimation. Biomech. Model Mechanobiol. 15, 1699–1712.
Goel, V.K., Winterbottom, J.M., Weinstein, J.N., Kim, Y.E., 1987. Load sharing among spinal elements of a motion segment in extension and lateral bending. J. Biomech. Eng. 109, 291–297.
Heuer, F., Schmidt, H., Claes, L., Wilke, H.-J., 2007a. Stepwise reduction of functional spinal structures increase vertebral translation and intradiscal pressure. J. Biomech. 40, 795–803.
Heuer, F., Schmidt, H., Klezl, Z., Claes, L., Wilke, H.-J., 2007. Stepwise reduction of functional spinal structures increase range of motion and change lordosis angle. J. Biomech. 40, 271–280.
Kingma, I., Faber, G.S., van Dieen, J.H., 2016. Supporting the upper body with the hand on the thigh reduces back loading during lifting. J. Biomech. 49, 881–889.
Lin, H.S., Liu, Y.K., Adams, K.H., 1978. Mechanical response of the lumbar intervertebral joint under physiological (complex) loading. J. Bone Joint Surg. Am. 60, 41–55.
Liu, T., Khalaf, K., Naserkhaki, S., El-Rich, M., 2018. Load-sharing in the lumbosacral spine in neutral standing & flexed postures - A combined finite element and inverse static study. J. Biomech. 70, 43–50.
Myklebust, J.B., Pintar, F., Yoganandan, N., Cusick, J.F., Maiman, D., Myers, T.J., Sances, A., 1988. Tensile strength of spinal ligaments. Spine 13, 526–531.
Naserkhaki, S., El-Rich, M., 2017. Sensitivity of lumbar spine response to follower load and flexion moment: finite element study. Comput. Methods Biomech. Biomed. Eng. 20, 550–557.
Naserkhaki, S., Jaremko, J.L., Adeeb, S., El-Rich, M., 2016. On the load-sharing along the ligamentous lumbosacral spine in flexed and extended postures: Finite element study. J. Biomech. 49, 974–982.
Nolte, L.P., Pingel, T.H., 1991. A planar nonlinear model of the human spine. Biomed. Tech. 36, 298–304.
O'Reilly, O.M., Metzger, M.F., Buckley, J.M., Moody, D.A., Lotz, J.C., 2009. On the stiffness matrix of the intervertebral joint: Application to total disk replacement. J. Biomech. Eng. 131.
Panjabi, M.M., Brand Jr., R.A., White 3rd, A.A., 1976. Three-dimensional flexibility and stiffness properties of the human thoracic spine. J. Biomech. 9, 185–192.
Panjabi, M.M., Krag, M.H., White Iii, A.A., Southwick, W.O., 1977. Effects of preload on load displacement curves of the lumbar spine. Orthop. Clin. North Am. 8, 181–192.
Panjabi, M.M., Oxland, T.R., Yamamoto, I., Crisco, J.J., 1994. Mechanical behavior of the human lumbar and lumbosacral spine as shown by three-dimensional load-displacement curves. J. Bone Joint Surg. 76, 413–424.
Patwardhan, A.G., Havey, R.M., Carandang, G., Simonds, J., Voronov, L.I., Ghanayem, A.J., Meade, K.P., Gavin, T.M., Paxinos, O., 2003. Effect of compressive follower preload on the flexionâ€“extension response of the human lumbar spine. J. Orthop. Res. 21, 540–546.
Patwardhan, A.G., Havey, R.M., Meade, K.P., Lee, B., Dunlap, B., 1999. A follower load increases the load-carrying capacity of the lumbar spine in compression. Spine 24, 1003–1009.
Pingel, T.H., 1991. Beitrag zur Herleitung und numerischen Realisierung eines mathematischen Modells der menschlichen Wirbelsäule. Mitteilungen aus dem Institut für Mechanik IfM 77, 95–106.
Sato, K., Kikuchi, S., Yonezawa, T., 1999. In vivo intradiscal pressure measurement in healthy individuals and in patients with ongoing back problems. Spine 24, 2468–2474.
Schmidt, H., Heuer, F., Drumm, J., Klezl, Z., Claes, L., Wilke, H.-J., 2007. Application of a calibration method provides more realistic results for a finite element model of a lumbar spinal segment. Clin. Biomech. (Bristol, Avon) 22, 377–384.
Schmidt, H., Heuer, F., Simon, U., Kettler, A., Rohlmann, A., Claes, L., Wilke, H.J., 2006. Application of a new calibration method for a three-dimensional finite element model of a human lumbar annulus fibrosus. Clin. Biomech. (Bristol, Avon) 21, 337–344.
Senteler, M., Weisse, B., Rothenfluh, D.A., Snedeker, J.G., 2015. Intervertebral reaction force prediction using an enhanced assembly of OpenSim models. Comput. Methods Biomech. Biomed. Eng., 1–11
Shirazi-Adl, A., 1988. Finite element stress analysis of disc annulus using different composite material models. New York, NY, United States.
Shirazi-Adl, A., Ahmed, A.M., Shrivastava, S.C., 1986. A finite element study of a lumbar motion segment subjected to pure sagittal plane moments. J. Biomech. 19, 331–350.
Shirazi-Adl, A., Parnianpour, M., 2000. Load-bearing and stress analysis of the human spine under a novel wrapping compression loading. Clin. Biomech. (Bristol, Avon) 15, 718–725.
Shirazi-Adl, S.A., Shrivastava, S.C., Ahmed, A.M., 1984. Stress analysis of the lumbar disc-body unit in compression. A three-dimensional nonlinear finite element study. Spine 9, 120–134.
Simulia, 2016. Abaqus Analysis User's Guide. 3DS Dassault Systems.
Stokes, I.A., Gardner-Morse, M., Churchill, D., Laible, J.P., 2002. Measurement of a spinal motion segment stiffness matrix. J. Biomech. 35, 517–521.
Takahashi, I., Kikuchi, S.-I., Sato, K., Sato, N., 2006. Mechanical load of the lumbar spine during forward bending motion of the trunk-a biomechanical study. Spine 31, 18–23.
Wang, S., Park, W.M., Kim, Y.H., Cha, T., Wood, K., Li, G., 2014. In vivo loads in the lumbar L3–4 disc during a weight lifting extension. Clin. Biomech. (Bristol, Avon) 29, 155–160.
Weisse, B., Aiyangar, A.K., Affolter, C., Gander, R., Terrasi, G.P., Ploeg, H., 2012. Determination of the translational and rotational stiffnesses of an L4–L5 functional spinal unit using a specimen-specific finite element model. J. Mech. Behav. Biomed. Mater. 13, 45–61.
Wilke, H.-J., Neef, P., Hinz, B., Seidel, H., Claes, L., 2001. Intradiscal pressure together with anthropometric data - a data set for the validation of models. Clin. Biomech. (Bristol, Avon) 16 (Suppl 1), S111–S126.
Wilke, Hans–Joachim, Neef, Peter, Caimi, Marco, Hoogland, Thomas, Claes, Lutz E., 1999. New in vivo measurements of pressures in the intervertebral disc in daily life. Spine 24 (8), 755–762. https://doi.org/10.1097/00007632-199904150-00005.
Wu, M., Wang, S., Driscoll, S.J., Cha, T.D., Wood, K.B., Li, G., 2014. Dynamic motion characteristics of the lower lumbar spine: implication to lumbar pathology and surgical treatment. Eur. Spine J. 23, 2350–2358.
Zander, T., Dreischarf, M., Timm, A.K., Baumann, W.W., Schmidt, H., 2017. Impact of material and morphological parameters on the mechanical response of the lumbar spine - A finite element sensitivity study. J. Biomech. 53, 185–190.
Zanjani-Pour, S., Meakin, J.R., Breen, A., Breen, A., 2018. Estimation of in vivo inter-vertebral loading during motion using fluoroscopic and magnetic resonance image informed finite element models. J. Biomech. 70, 134–139.
Nolte, L.P., Panjabi, M.M., Oxland, T.R., 1990. Biomechanical properties of lumbar spinal ligaments in book of Clinical implant materials by Heimke. In: Advances in Biomaterials. Elsevier Science Publishers B.V., Amsterdam, The Netherlands, pp. 663–668.